Journal of Advanced Marine Engineering and Technology, Vol. 50, No. 5, pp. 374~381, 2026
J. Advanced Marine Engineering and Technology (JAMET)
https://doi.org/10.5916/jamet.2026.50.5.374

ISSN 2234-7925 (Print)
ISSN 2765-4796 (Online)
Original Paper

System-level validation of CFD-informed linear-quadratic hydrodynamic damping for the VolturnUS-S floating wind turbine under controller-off conditions

Hyeon-Gyu Kim[1] · Hyeon-Gyo Chae[2] · Chan Roh†

(Received September 29, 2026 ; Revised October 15, 2026 ; Accepted October 27, 2026)

Abstract: This study validates a computational-fluid-dynamics-informed linear-quadratic (CFD-LQ) hydrodynamic damping model at the system level for the IEA 15 MW wind turbine mounted on the UMaine VolturnUS-S semisubmersible platform. Turbine control, wind, and current were disabled to isolate the hydrodynamic contribution. OpenFAST free-decay tests with initial pitch perturbations of 1, 2, 5, and 7 deg yielded damping ratios of 0.374-1.245% for the IEA baseline damping model and 2.319-2.643% for the CFD-LQ model. The damped natural period remained approximately 28.74 s, indicating that the model change primarily modified energy dissipation rather than restoring behavior. At a measured regular-wave period of 29.143 s, the pitch response-amplitude operator decreased from 5.985 to 3.470 deg/m, corresponding to a 42.0% reduction. The half-power bandwidth increased by 47.6%, and the approximate quality factor decreased by 32.0%. Hydrodynamic, hydrostatic, tower-base, and mooring responses exhibited consistent reductions near resonance. An independent resonance-band dataset produced a 42.8% pitch-response reduction at 29.032 s among the independently generated wave conditions. Agreement between decay-based and forced-response evidence demonstrates that, within the tested amplitude range, the CFD-LQ prescription increases viscous dissipation without materially shifting the system resonance. The study also identifies wave-frequency discretization as a critical source of false resolution in narrow-band RAO scans.

Keywords: Floating offshore wind turbine; OpenFAST; CFD-informed correction; Hydrodynamic damping; Free decay; Response-amplitude operator

1. Introduction

Floating offshore wind turbines are dynamically coupled systems in which the rotor-nacelle assembly, support structure, platform, moorings, waves, wind, and controller interact. For semisubmersible concepts, low-frequency platform pitch can amplify tower and blade loads, modulate mooring tension, and change rotor inflow. The IEA 15 MW reference turbine and the UMaine VolturnUS-S platform provide a reproducible basis for studying these interactions **[1][2]**, while OpenFAST supplies the coupled time-domain framework **[3]**.

Potential-flow radiation and diffraction models, even when combined with Morison loading, may underrepresent dissipation caused by separation, vortex shedding, and other viscous mechanisms. Underpredicted damping leads directly to overpredicted resonant motion and load transfer. Previous calibration studies have also shown that damping or drag coefficients inferred from one excitation regime need not remain optimal in another **[4]**. High-fidelity CFD, including CFD coupled directly with OpenFAST, has therefore been used to resolve these viscous effects at the platform level **[5]**. A defensible correction must therefore preserve restoring behavior, increase decay consistently over a useful amplitude range, and reduce forced response near resonance without relying on nominal input labels alone.

This work evaluates a predefined CFD-informed linear-quadratic damping model after its implementation in OpenFAST. The contribution is not a new CFD coefficient-identification procedure. Instead, system-level evidence is assembled from four free-decay amplitudes, a broad regular-wave sweep, and an independently executed resonance-band sweep. The measured wave elevation is used to recover the actual forcing period and

† Corresponding Author (ORCID: https://orcid.org/0000-0003-1407-4812): Associate Professor, Division of Marine System Engineering, Korea Maritime & Ocean University, 727, Taejong-ro, Yeongdo-gu, Busan 49112, Korea, E-mail: rohchan@kmou.ac.kr, Tel: 051-405-4285
1 M. S. Candidate, Division of Marine System Engineering, Korea Maritime & Ocean University, E-mail: kimg9706@naver.com
2 Ph. D. Candidate, Division of Marine System Engineering, Korea Maritime & Ocean University, E-mail: chae@g.kmou.ac.kr

This is an Open Access article distributed under the terms of the Creative Commons Attribution Non-Commercial License (http://creativecommons.org/licenses/by-nc/3.0), which permits unrestricted non-commercial use, distribution, and reproduction in any medium, provided the original work is properly cited.

Copyright ⓒ The Korean Society of Marine Engineering

amplitude. Platform motion, hydrodynamic moment, structural response, and mooring tension are then examined using one consistent harmonic-regression procedure.

2. Numerical Model and Analysis Procedure

2.1 System Definition and Isolated Hydrodynamic Condition

The system comprises the IEA 15 MW reference wind turbine and the UMaine VolturnUS-S semisubmersible **[1][2]**. Time-domain simulations were performed with OpenFAST **[3]**, the successor of FAST **[6]**. The baseline (BASE) and corrected (CFD-LQ) cases use identical mass, hydrostatic restoring, and mooring definitions. Wind speed and current speed are zero, and the turbine controller is disabled. Consequently, the comparison isolates the hydrodynamic-model contribution and must not be interpreted as a validation of the Reference OpenSource Controller (ROSCO) or operating-turbine control performance. A regular-wave amplitude of approximately 0.5 m was used as a common fixed-excitation condition so that the BASE and CFD-LQ models could be compared without changing the forcing level. This amplitude is an analysis choice, not an identified threshold for nonlinear damping or a representative design-sea state; amplitude sensitivity remains outside the present regular-wave matrix. The numerical conditions are summarized in **Table 1**.

2.2 CFD-Informed Linear-Quadratic Damping

The BASE and CFD-LQ cases use alternative pitch-damping prescriptions while retaining identical mass, hydrostatic-restoring, radiation, Morison-member, and mooring definitions. Platform degrees of freedom are ordered as surge, sway, heave, roll, pitch, and yaw; therefore, the pitch terms are entered at matrix location (5,5). For pitch, the added damping moment is written as **Equation (1)**:

$$M_d = -B_{\mathrm{lin}}\dot{\theta} - B_{\mathrm{quad}}\left|\dot{\theta}\right|\dot{\theta} \tag{1}$$

where B_{lin} is the equivalent linear coefficient and B_{quad} represents amplitude-dependent dissipation. The IEA baseline case uses AddBLin(5,5) = 0 and AddBQuad(5,5) = 1.676×10^{10} N·m·s²/rad². The CFD-LQ case uses AddBLin(5,5) = 5.65×10^{8} N·m·s/rad and AddBQuad(5,5) = 7.88×10^{8} N·m·s²/rad². All other entries of the added damping matrices are zero. These values were taken from the CFD-based model configuration evaluated in this study; they were not re-identified from the present OpenFAST responses. Because stiffness, mass, and mooring properties are unchanged, a nearly unchanged natural period together with faster decay is the expected signature of a damping-dominant model change. In principle, a linear-quadratic representation can be calibrated by resolving CFD-derived pitch moment and angular-velocity histories and separating contributions proportional to angular velocity and to its magnitude multiplied by angular velocity. However, the underlying CFD fitting records and their identification details are not included in the present dataset; therefore, this study assesses the system-level consequences of the specified coefficients, not the uniqueness or accuracy of their original CFD identification.

Table 1: Numerical conditions used in the model comparison

Item	Setting
System	IEA 15 MW + VolturnUS-S
Cases	BASE and CFD-LQ
Controller / wind / current	OFF / 0 m/s / 0 m/s
Regular wave	Head sea; amplitude about 0.5 m
Full-band sweep	8-45 s (nominal)
Refined sweep	27.0-31.0 s, 0.5 s step (nominal)
Narrow-band sweep	28.4-30.0 s, 0.2 s step (nominal)
Steady-state window	900-1800 s
Free decay	+1, +2, +5, +7 deg; 1500 s
Time step	0.025 s

2.3 Decay Identification and Harmonic Regression

The static pitch equilibrium was approximately −1.442 deg. The prescribed initial pitch values are relative perturbations about this equilibrium. Positive and negative peaks were treated separately, and log-amplitude was regressed against time. For successive same-direction peaks x_k and x_{k+1}, the logarithmic decrement and damping ratio are obtained from **Equation (2)**:

$$\delta = \ln\left(\frac{x_k}{x_{k+1}}\right), \quad \zeta = \frac{\delta}{\sqrt{(2\pi)^2+\delta^2}} \tag{2}$$

For regular-wave cases, each steady-state response y(t) was represented by a mean, a linear trend, and a harmonic component, as in **Equation (3)**, and the response-amplitude operator (RAO) was obtained from the harmonic amplitudes using **Equation (4)**:

$$y(t) = c_0 + c_1 t + a\cos\omega t + b\sin\omega t \tag{3}$$

$$\mathrm{RAO} = \frac{A_y}{A_\eta} = \frac{\sqrt{a^2+b^2}}{A_\eta} \tag{4}$$

where ω is the identified wave angular frequency, a and b are the regression coefficients, and A_η is the wave amplitude obtained by applying the same regression to the wave-elevation channel Wave1Elev (m). The actual wave period was selected by maximizing the harmonic-fit coefficient of determination for Wave1Elev. This step prevents nominal filenames from introducing frequency error into a narrow resonance scan.

Because SeaState discretizes wave frequencies, the realized wave period can differ from the nominally requested period, and adjacent nominal periods can yield identical wave records. Therefore, the forcing periods used in the RAO analysis were determined from Wave1Elev rather than from nominal input labels. The four distinct periods in the independent narrow-band dataset are consistent with a frequency spacing of approximately 1/1800 Hz; this spacing is not assumed for the refined sweep.

2.4 Resonance Bandwidth and Equivalent Oscillator Identification

Two complementary frequency-domain indicators were added. First, the half-power period limits were obtained by linear interpolation at $RAO_{max}/\sqrt{2}$ on both sides of the measured peak. The corresponding frequency-domain quality factor was evaluated using **Equation (5)**:

$$Q = \frac{f_p}{f_2 - f_1} \tag{5}$$

where f_p is the peak frequency and f_1 and f_2 are the half-power frequencies. Because the period grid is finite, these quantities are approximate comparative metrics rather than exact modal parameters. Second, the measured amplitude and phase were fitted simultaneously using the equivalent single-degree-of-freedom (SDOF) response in **Equations (6)** and **(7)**, where $r = \omega/\omega_n$:

$$H(\omega) = \frac{K}{\sqrt{(1-r^2)^2 + (2\zeta r)^2}} \tag{6}$$

$$\phi(\omega) = \phi_0 - \operatorname{atan2}(2\zeta r,\ 1 - r^2) \tag{7}$$

In **Equations (6)** and **(7)**, K is the quasi-static gain and ϕ_0 is the excitation phase. The four parameters K, ζ, ω_n, and ϕ_0 were identified by nonlinear least squares using the refined sweep and the four independently generated narrow-band conditions. The fit is used to interpret resonance sharpness and to estimate a model-dependent peak between sampled periods. The directly simulated reduction remains the primary quantitative evidence for the system-level assessment.

3. Results

3.1 Free-Decay Response and Amplitude Dependence

As shown in **Figure 1**, the BASE responses retain visible oscillation throughout the 1500 s records, whereas the CFD-LQ responses converge rapidly toward equilibrium. In the last 200 s, the peak-to-peak pitch amplitude decreased from 0.844 (BASE) to 0.0027 deg (CFD-LQ) for the 1 deg test and from 1.333 to 0.0122 deg for the 7 deg test. The correction therefore remains effective across the tested disturbance range. Initial perturbations of 1, 2, 5, and 7 deg were chosen to sample small through comparatively large pitch departures from the static equilibrium within the investigated sub-crossover range (Section 4), rather than to represent a statistical distribution of operating conditions. The four levels permit a direct check of amplitude-dependent decay without altering the model parameters.

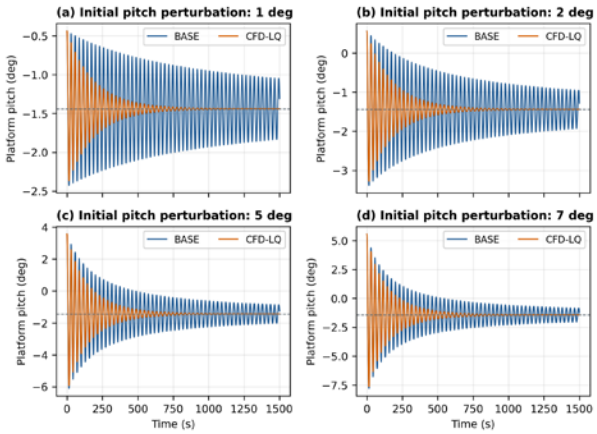

Figure 1: Pitch free-decay responses for four initial perturbations

Table 2: Identified pitch-decay metrics

Init.	Case	T_d (s)	ζ (%)	$t_{1/2}$ (s)
1°	BASE	28.738	0.374	846.9
1°	CFD-LQ	28.747	2.319	136.7
2°	BASE	28.735	0.659	481.3
2°	CFD-LQ	28.746	2.416	131.2
5°	BASE	28.734	1.163	272.5
5°	CFD-LQ	28.745	2.618	121.1
7°	BASE	28.734	1.245	254.6
7°	CFD-LQ	28.746	2.643	119.9

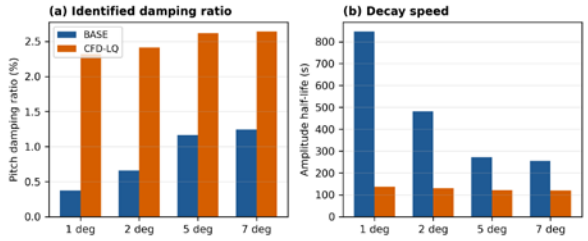

Figure 2: Damping ratio and amplitude half-life identified from free decay.

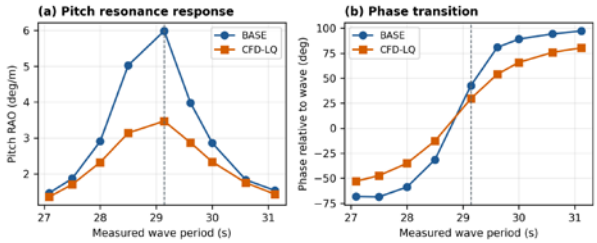

Figure 4: Pitch RAO and response phase based on measured wave periods

Table 2 and **Figure 2** summarize the decay metrics. The damping-ratio multiplier is 6.20, 3.67, 2.25, and 2.12 for the 1, 2, 5, and 7 deg tests, respectively. The corresponding half-life reduction is 83.9%, 72.7%, 55.6%, and 52.9%. Linear fits against initial amplitude give slopes of 0.146 percentage points/deg for BASE and 0.055 percentage points/deg for CFD-LQ ($R^2 \approx 0.94$ for both). Thus, the absolute damping remains amplitude dependent, but its coefficient of variation across the tested amplitudes drops from 48.2% to 6.3% after correction. Meanwhile, the natural-period coefficient of variation is only 0.0066% for BASE and 0.0028% for CFD-LQ, and the model-to-model period shift remains about 0.04%. These results support a dissipation change rather than an unintended stiffness change.

3.2 Full-band Response and Modal Selectivity

The full-band sweep from 8 to 45 s (**Figure 3**) places the pitch result in a broader modal context. The largest surge response occurs at 45 s and is 1.816 m/m for both models. The heave peak occurs at 22 s and changes only from 1.5474 to 1.5478 m/m. In contrast, the pitch peak at the full-band sample nearest 29 s decreases from 6.021 to 3.478 deg/m, or 42.2%. The correction is therefore strongly selective around the pitch-dominated resonance and does not introduce a comparable change in the principal surge or heave peaks. This selectivity is consistent with the prescribed damping formulation and reduces concern that the model is globally overdamped.

3.3 Refined Pitch Resonance and Bandwidth

The measured period of the refined-sweep condition nominally labeled 29.0 s was 29.143 s. Using the nominal period gave an input-wave fit of $R^2 = 0.926$, whereas using the measured period increased it to 0.99999. At 29.143 s, the pitch RAO decreased from 5.985 to 3.470 deg/m, or 42.0%. The resonance location was retained while the peak was suppressed, consistent with the free-decay evidence. Because this 42.0% decrease was obtained for approximately 0.5 m regular-wave amplitude, it should not be assumed invariant with wave amplitude. The quadratic damping term makes the effective damping amplitude dependent, so the quantitative reduction at other wave amplitudes requires additional simulations. **Figure 4** presents the measured-period pitch RAO and phase.

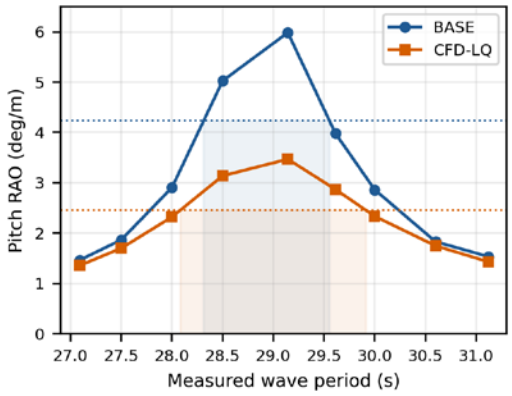

Figure 5: Approximate half-power bandwidth of the measured pitch RAO

Table 3: Approximate resonance-band metrics from the refined sweep

Metric	BASE	CFD-LQ	Change
Peak period (s)	29.143	29.143	0.0%
Peak RAO (deg/m)	5.985	3.470	−42.0%
Half-power width (s)	1.241	1.832	+47.6%
Quality factor Q	23.14	15.73	−32.0%

Linear interpolation at the half-power level (**Figure 5** and **Table 3**) gives a period-bandwidth increase from 1.241 to 1.832 s, while the approximate quality factor decreases from 23.14 to 15.73. The 47.6% wider resonance band and 32.0% lower Q quantitatively confirm that CFD-LQ suppresses a narrow, high-amplification mode rather than merely shifting the sampled maximum. These bandwidth values are comparative because the forcing grid remains coarse relative to the resonance width.

3.4 Independent Resonance-Band Repeatability

The independent narrow-band runs were nominally assigned from 28.4 to 30.0 s at 0.2 s spacing. Wave1Elev and file-hash checks, however, showed that adjacent requests generated identical waves because of SeaState frequency discretization. The nine labels therefore reduce to four independent measured periods: 28.571, 29.032, 29.508, and 30.000 s. Treating duplicates as separate observations would create false frequency resolution and artificially inflate the apparent sample size. **Table 4** and **Figure 6** present the responses for these four measured periods. Nominal 0.2 s period increments yielded only four distinct measured periods because of SeaState frequency discretization.

Among the independently generated conditions, the largest BASE response occurred at 29.032 s and was reduced by 42.8% with CFD-LQ. This differs by only 0.8 percentage points from the 42.0% reduction at 29.143 s in the refined sweep. The reduction is therefore reproducible across two executions, but 29.032 s should be described only as the maximum among the evaluated conditions, not as an exactly identified resonance period. A half-window convergence check was below 0.4% for most pitch-RAO cases; the BASE result at 30.0 s differed by approximately 9%, indicating slower convergence on the descending branch and motivating a longer record for future refinement.

3.5 Equivalent Oscillator Interpretation

Figure 7 and **Table 5** summarize the equivalent-oscillator fit. The fitted natural periods differ by less than 0.1% and remain within 0.7% of the 28.74 s free-decay period. The equivalent damping ratio rises from 1.263% to 2.870%, while the interpolated SDOF peak decreases by 54.2%. This model-based peak reduction is larger than the directly sampled 42.0-42.8% because the low-damped BASE peak is sharper and lies between discrete wave periods. The BASE amplitude-fit error of 8.45%, compared with 1.70% for CFD-LQ, also indicates stronger nonlinearity or incomplete steady-state convergence in the lightly damped case. Accordingly, 42% is retained as the directly demonstrated reduction, while 54% is reported only as an equivalent-linear estimate. These fit errors describe model-to-data agreement within the evaluated sweep; they should not be interpreted as uncertainty bounds on the nonlinear damping coefficients.

Table 4: Independent resonance-band pitch RAO

T (s)	BASE	CFD-LQ	Reduction
28.571	5.319	3.244	39.0%
29.032	6.170	3.529	42.8%
29.508	4.401	3.022	31.3%
30.000	2.862	2.335	18.4%

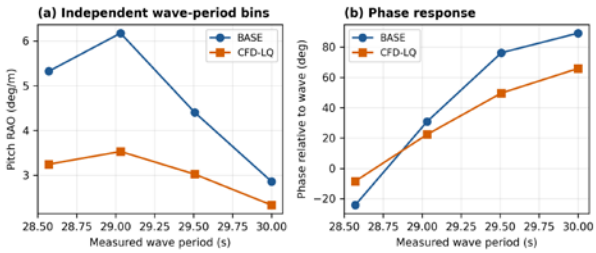

Figure 6: Independent measured-period RAO and phase response

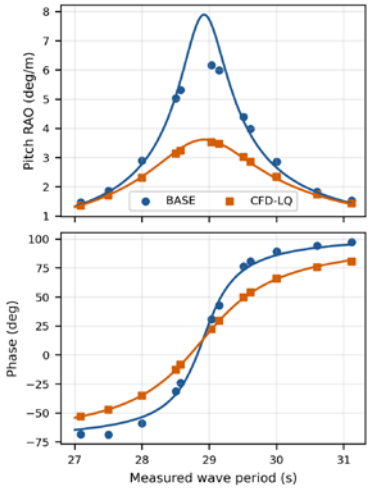

Figure 7: Equivalent oscillator fit to the combined pitch RAO and phase data

Table 5: Equivalent oscillator parameters identified from regular-wave responses. Amplitude RMS error quantifies the RMS discrepancy of fitted versus simulated RAO amplitude (reported in %); phase RMS error is the RMS phase discrepancy (degrees)

Parameter	BASE	CFD-LQ	Interpretation
T_n (s)	28.917	28.900	Difference <0.1%
Equivalent ζ (%)	1.263	2.870	2.27-fold
Estimated peak RAO (deg/m)	7.893	3.616	−54.2%
Amplitude RMS error	8.45%	1.70%	BASE less linear
Phase RMS error	3.90°	0.54°	CFD-LQ near SDOF

3.6 Transfer to Hydrodynamic, Structural, and Mooring Loads

Figure 8 and **Table 6** show that pitch-motion suppression propagates consistently to the hydrodynamic moment and principal structural responses. Across the seven listed response metrics, the mean reduction is 40.7% with a standard deviation of 3.3 percentage points. Fairlead and anchor tensions decrease by 43.1% and 33.5%, respectively, at the measured resonance condition. Post-resonance mooring RAOs can nevertheless exceed the BASE values at some periods, indicating phase redistribution rather than uniform attenuation across the full frequency range.

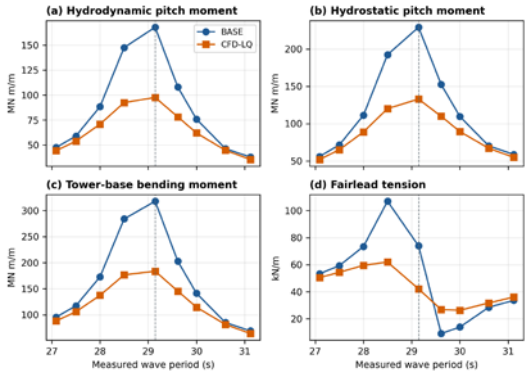

Figure 8: Hydrodynamic, structural, and mooring-load RAOs near pitch resonance

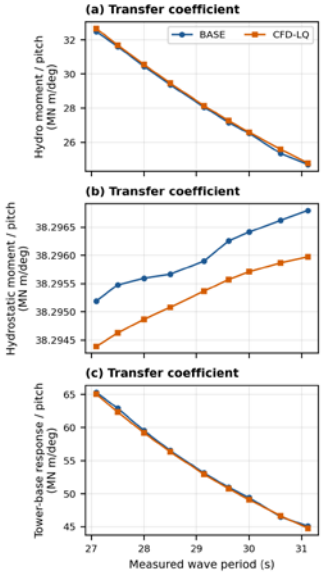

Figure 9: Motion-normalized hydrodynamic and structural response coefficients. Panels (a), (b), and (c) show the hydrodynamic moment (HydroMyi), hydrostatic moment (B1HDSMyi), and tower-base bending moment (TwrBsMyt), respectively, each normalized by pitch response amplitude (MN·m/deg)

Table 6: Response metrics at the measured period of 29.143 s

Response	BASE	CFD-LQ	Reduction
Pitch (deg/m)	5.985	3.470	42.0%
HydroMyi (MN·m/m)	167.96	97.65	41.9%
B1HDSMyi (MN·m/m)	229.21	132.89	42.0%
B1RdtMyi (MN·m/m)	62.75	37.39	40.4%
TwrBsMyt (MN·m/m)	317.95	183.72	42.2%
FairTen1 (kN/m)	73.94	42.08	43.1%
AnchTen1 (kN/m)	51.17	34.03	33.5%

OpenFAST channel definitions: HydroMyi is the total hydrodynamic moment about the global y-axis; B1HDSMyi is the body-1 hydrostatic moment about the global y-axis; B1RdtMyi is the body-1 radiation-memory moment about the global y-axis; TwrBsMyt is the tower-base fore-aft bending moment; FairTen1 and AnchTen1 are the fairlead and anchor tensions of mooring line 1, respectively. Moment RAOs are reported in MN·m/m and tension RAOs in kN/m, normalized by wave amplitude.

Regressing each load RAO against pitch RAO (Figure 9) over the refined band gives nearly unchanged slopes for the principal pitch-mediated quantities. HydroMyi changes from 28.31 to 28.04 MN·m/deg, B1HDSMyi from 38.296 to 38.295 MN·m/deg, and TwrBsMyt from 53.52 to 52.33 MN·m/deg. The B1HDSMyi relation is essentially exact ($R^2 > 0.999999$), while HydroMyi and TwrBsMyt retain R^2 values above 0.91. The load-transfer path is therefore almost unchanged; the approximately 42% load reduction is primarily the consequence of reduced platform pitch amplitude. Mooring tension is less directly proportional to pitch because surge coupling and line dynamics redistribute phase and amplitude.

4. Discussion

Free decay and forced response provide mutually reinforcing evidence. The former shows a two- to six-fold increase in damping ratio without a material period shift. The latter shows nearly identical directly sampled resonance-reduction estimates in two separately executed datasets, together with a wider half-power band, a lower quality factor, and comparable reductions in hydrodynamic and structural response. This cross-domain agreement is stronger than a curve fit to one response trace because the decay envelope, resonance sharpness, phase transition, and load-transfer path respond consistently to the same model change.

The amplitude dependence is consistent with the two damping prescriptions. The CFD-LQ case replaces the large baseline quadratic coefficient with a dominant linear term and a much

smaller quadratic term; therefore, the damping difference $\zeta_{CFD\text{-}LQ}-\zeta_{BASE}$ is expected to shrink as the response amplitude increases, as observed (1.945 percentage points at 1 deg and 1.398 percentage points at 7 deg). Under harmonic equivalent linearization, a quadratic coefficient B_{quad} contributes an equivalent linear damping of $8\omega_n A B_{quad}/(3\pi)$ at pitch amplitude A. With $\omega_n = 2\pi/28.74$ s, the added-term damping of CFD-LQ exceeds that of BASE by factors of approximately 10.5, 5.3, 2.1, and 1.5 at 1, 2, 5, and 7 deg, respectively. These factors follow the same trend as the identified multipliers of 6.20, 3.67, 2.25, and 2.12, which are smaller at low amplitude because both cases share the same radiation and Morison damping. Equating the two added-damping terms gives the crossover amplitude in **Equation (8)**:

$$A^* = \frac{3\pi B_{\text{lin}}^{\text{CFD}}}{8\,\omega_n\left(B_{\text{quad}}^{\text{BASE}} - B_{\text{quad}}^{\text{CFD}}\right)} \tag{8}$$

which yields $A^* \approx 0.191$ rad (10.9 deg). Above this amplitude, the BASE prescription would dissipate more energy than CFD-LQ. The present conclusions are therefore limited to pitch amplitudes below the crossover; all evaluated responses satisfy this condition (maximum initial perturbation of 7 deg and maximum regular-wave response of approximately 3 deg). Moreover, the whole-record log-decrement fit provides trajectory-averaged values rather than matched-amplitude coefficients. A cycle-wise p-q identification, which regresses the logarithmic decrement against the mean cycle amplitude, should be used to separate the linear and quadratic contributions directly.

In this study, system-level validation is limited to assessing the consistency of the specified damping correction across free-decay and regular-wave responses. It does not establish the accuracy of the underlying CFD-derived coefficients against physical experiments or validate performance under operating control. The controller-off design is valuable because it removes aerodynamic and control-induced damping, but full-system application requires additional checks under turbulent wind, irregular waves, and controller activation. Morison drag coefficients were held unchanged between the two cases; consequently, the results demonstrate the system-level effects of the implemented damping prescription but do not independently eliminate possible overlap between Morison dissipation and the CFD-informed added terms. Accordingly, the correction should be treated as a site- and response-regime-dependent model input whose calibration and possible overlap with existing Morison damping require verification before design-level use.

The frequency-discretization finding is also methodologically important. A nominal 0.2 s input grid did not produce nine independent waves. The four measured periods in the independent narrow-band dataset are consistent with a frequency grid of approximately 1/1800 Hz, which gives a local period resolution $\Delta T \approx T^2\Delta f \approx 0.47$ s near 29 s. Increasing the SeaState repeat period to 3600 or 7200 s would improve the theoretical local resolution to approximately 0.23 or 0.12 s, respectively. Each run should still be accepted only after checking Wave1Elev and after the full-window and half-window RAOs converge.

The strongest next validation is the planned wave-amplitude matrix at 0.25, 0.50, and 1.00 m amplitude. It should report RAO, phase, cycle-wise damping, and the normalized load-to-motion gains used here. This matrix will determine whether the quadratic term produces the expected increase in equivalent damping with response amplitude. Subsequent irregular-wave cases should compare power spectral density (PSD), root-mean-square (RMS) values, maxima, and fatigue-equivalent loads, followed by ROSCO OFF/ON cases to quantify the interaction between hydrodynamic, aerodynamic, and control-induced damping. These additional simulations are proposed as future validation rather than as evidence already established by the present single-amplitude regular-wave tests.

5. Conclusions

A CFD-informed linear-quadratic hydrodynamic damping correction was evaluated for the IEA 15 MW–VolturnUS-S system under controller-off, zero-wind, and zero-current conditions. The principal findings are as follows.

1. Across 1-7 deg free-decay tests, the damping ratio increased from 0.374-1.245% for BASE to 2.319-2.643% for CFD-LQ, while the damped period remained approximately 28.74 s.
2. The amplitude half-life decreased by 52.9-83.9%, and damping variability over the tested amplitudes was substantially reduced because the dominant linear term replaced most of the baseline quadratic damping; the two prescriptions are expected to give equal added damping near 10.9 deg.
3. At the measured wave period of 29.143 s, the pitch RAO decreased by 42.0%; an independent dataset gave a 42.8% reduction at 29.032 s among the evaluated conditions.

4. The half-power period width increased by 47.6% and the approximate quality factor decreased by 32.0%, quantifying the reduction in resonance sharpness.
5. An equivalent-oscillator fit estimated damping ratios of 1.263% and 2.870% and a 54.2% interpolated peak reduction; because the BASE fit error was 8.45%, the directly simulated 42% remains the primary claim.
6. Hydrodynamic, hydrostatic, radiation-memory, tower-base, and mooring responses decreased consistently near resonance, with a mean reduction of 40.7% across seven metrics; principal load-to-pitch gains changed by less than about 2.3%.

The correction selectively suppresses the pitch-dominated resonance without materially changing surge and heave peaks or restoring characteristics, but frequency discretization and off-resonance mooring-phase effects must be considered. For practical floating offshore wind turbine analysis, the CFD-LQ terms can be introduced as pitch-specific supplemental damping in HydroDyn and screened against the uncorrected model using free-decay and measured-period RAOs before evaluating coupled load responses. Application to design conditions should then be checked with irregular seas, operational wind, and active control; the present controller-off results are not a transferable 42% reduction guarantee.

Acknowledgement

This research was supported by the Ministry of Trade, Industry and Energy (MOTIE) and the Korea Evaluation Institute of Industrial Technology (KEIT), Republic of Korea (grant numbers RS-2024-00437087) and by the National Research Foundation of Korea (NRF) grant funded by the Korean government (Grant No. RS-2026-25478244).

Author Contributions

Conceptualization, C. Roh and H. G. Kim; Methodology, H. G. Kim and H. G. Chae; Software, H. G. Kim; Formal Analysis, H. G. Kim and H. G. Chae; Investigation, H. G. Kim; Resources, C. Roh; Data Curation, H. G. Kim; Writing–Original Draft Preparation, H. G. Kim; Writing–Review & Editing, H. G. Chae and C. Roh; Visualization, H. G. Kim; Supervision, C. Roh; Project Administration, C. Roh; Funding Acquisition, C. Roh.

References

[1] E. Gaertner, J. Rinker, L. Sethuraman, F. Zahle, B. Anderson, G. Barter, N. Abbas, F. Meng, P. Bortolotti, W. Skrzypinski, G. Scott, R. Feil, H. Bredmose, K. Dykes, M. Shields, C. Allen, and A. Viscelli, Definition of the IEA 15-Megawatt Offshore Reference Wind Turbine, Technical Report NREL/TP-5000-75698, National Renewable Energy Laboratory, USA, 2020.

[2] C. Allen, A. Viscelli, H. Dagher, A. Goupee, E. Gaertner, N. Abbas, M. Hall, and G. Barter, Definition of the UMaine VolturnUS-S Reference Platform Developed for the IEA Wind 15-Megawatt Offshore Reference Wind Turbine, Technical Report NREL/TP-5000-76773, National Renewable Energy Laboratory, USA, 2020.

[3] OpenFAST Documentation v4.1.2: HydroDyn and SeaState Input Files, https://openfast.readthedocs.io/, Accessed September 29, 2026.

[4] M. Böhm, A. Robertson, C. Hübler, R. Rolfes, and P. Schaumann, “Optimization-based calibration of hydrodynamic drag coefficients for a semisubmersible platform using experimental data of an irregular sea state,” Journal of Physics: Conference Series, vol. 1669, p. 012023, 2020. [Online]. Available: https://doi.org/10.1088/1742-6596/1669/1/012023

[5] G. Campaña-Alonso, R. Martín-San-Román, B. Méndez-López, P. Benito-Cia, and J. Azcona-Armendáriz, “OF^2: Coupling OpenFAST and OpenFOAM for high-fidelity aero-hydro-servo-elastic FOWT simulations,” Wind Energy Science, vol. 8, pp. 1597-1611, 2023. [Online]. Available: https://doi.org/10.5194/wes-8-1597-2023

[6] J. M. Jonkman and M. L. Buhl Jr., FAST User’s Guide, Technical Report NREL/EL-500-38230, National Renewable Energy Laboratory, USA, 2005.